

---

# From Single-Step Edit Response to Multi-Step Molecular Optimization

---

Haojie Rao<sup>†</sup>, Kun Li<sup>†</sup>, Yida Xiong, Jiameng Chen, and Wenbin Hu<sup>\*</sup>

School of Computer Science,  
Wuhan University  
Wuhan, China

{raohaojie, likun98, yidaxiong, jiameng.chen, hwb}@whu.edu.cn

<sup>†</sup>These authors contributed equally. <sup>\*</sup>Corresponding author.

**Yizhen Zheng**

Department of Data Science and Artificial Intelligence,  
Monash University  
Victoria, Australia

yizhen.zhengl@monash.edu

**Jiajun Yu**

College of Computer Science and Technology,  
Zhejiang University  
Hangzhou, China

jiajunyu1999@gmail.com

**Duanhua Cao**

School of Life Sciences and Technology,  
Tongji University  
Shanghai, 200092, China

caodh@tongji.edu.cn

## Abstract

Conditional molecular optimization aims to edit a molecule to realize a specified property shift. In practice, structurally similar molecule data is scarce, while decisions are inherently action-level: at each step, the system must select one local structural edit from a candidate set that is strictly filtered by chemical feasibility rules. This level mismatch between supervision and decision makes oracle-in-the-loop search unstable in molecular optimization. Regressing on property differences between molecule pairs improves data efficiency but relies on oracle-in-the-loop search, entangling transformation effects with global context and providing limited guidance for selecting the next feasible edit, often resorting to oracle-in-the-loop search. For this reason, we propose a response-oriented discrete edit optimization approach comprising two tightly coupled components: a single-step molecular edit response predictor (SMER) and a multi-step planner that composes local predictions into optimization trajectories via guided tree search (SMER-Opt). The approach learns a directional evaluation model over edit actions to support constraint-aware planning. It mines weakly related molecule pairs and decomposes their structural differences into minimal edit units, turning endpoint property annotations into process-level supervision and yielding reusable, transferable action primitives. A directional edit evaluator then scores feasible candidate edits by their likelihood of moving the molecule toward the desired property change, substantially reducing dependence on external evaluator queries at decision time. Code is available at <https://anonymous.4open.science/r/SMER>.

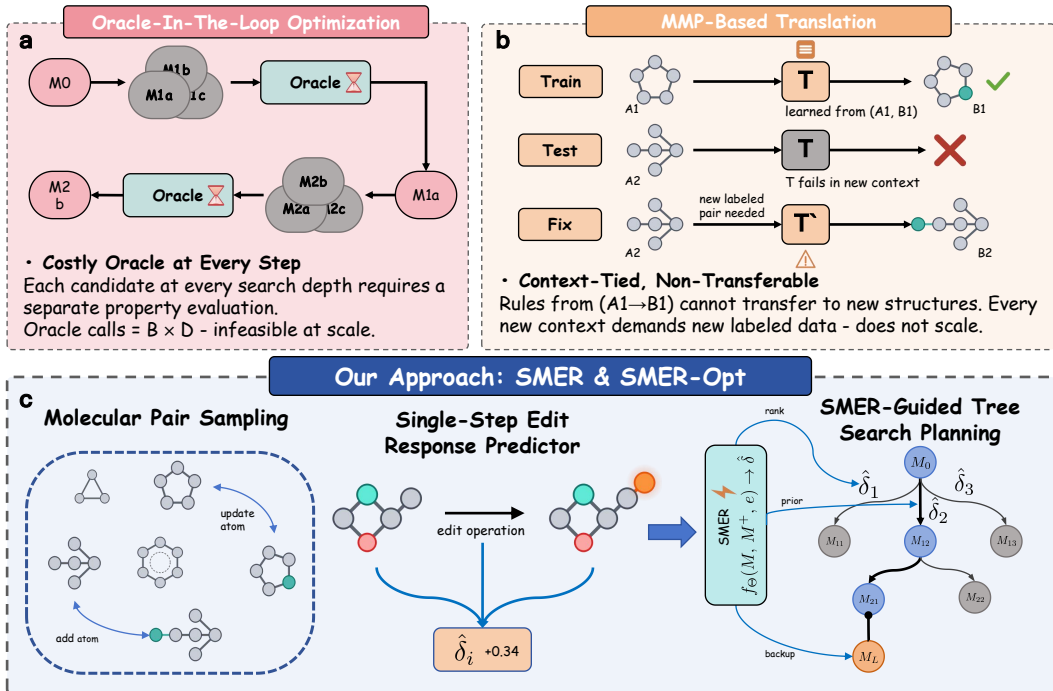


Figure 1: Comparison of molecular optimization approaches: (a) oracle-in-the-loop optimization, (b) MMP-based translation, and (c) our SMER & SMER-Opt.

## 1 Introduction

Molecular optimization seeks to improve a given molecule with respect to target objectives, such as physicochemical properties [46] and biological activity [3, 19], subject to chemical validity constraints [52]. The field has evolved through several distinct generations. Early approaches cast optimization as endpoint-scored search via graph reinforcement learning [49, 56] or latent-space traversal through variational autoencoders and flow models [13, 37]. To provide more explicit structural guidance, DST [8] introduced differentiable scaffold trees that enable gradient-based multi-step editing over predefined scaffolds. As the demand for richer optimization signals grew, DyMol [38] abandoned fixed scaffold assumptions and shifted guidance into continuous distribution space, framing optimization as distribution-level steering. The subsequent rise of large language models (LLMs) opened a new frontier [52, 53, 47, 21, 4]; CMOMO [45] further extends this generative paradigm to simultaneous multi-objective conditioning. In parallel, GFlowNets [1, 18, 14], diffusion-based [55, 28], and energy-based formulations [26, 27] have framed optimization as amortized sampling over chemical space. A complementary line casts optimization as structure translation guided by matched molecular pairs (MMP) [12], learning edit rules from structurally similar compounds that differ in the target property. Despite this breadth of innovation, these approaches collapse into two failure modes rooted in the absence of explicit edit-level guidance.

Oracle-in-the-loop optimizers such as graph learning [51, 22, 50], GFlowNets [1, 18, 14], diffusion [55, 28], and energy-based methods [26, 27] rely on oracle evaluations at every search step; this is costly under experimental budgets, and molecule-level rewards do not indicate which edit drove improvement. MMP-based translation methods learn edit rules from matched pairs, excluding many molecular relationships and yielding rules that generalize poorly to new scaffolds [31]. Both failure modes share a root: neither explicitly models **“which modification, applied where, shifts the objective by how much.”** Yet this edit-level signal is what optimization needs, since decisions are local and incremental while molecule-level supervision is sparse.

To address this gap, we take an edit-response view of molecular optimization: learn the property change  $\Delta y$  from minimal structural edits and compose feasible edits to approximate the target shift  $\Delta^*$ . Training signal is obtained by decomposing structurally related molecule pairs, turning endpoint labels into process-level supervision. SMER estimates each candidate edit’s property change, and

SMER-Opt combines local predictions with Monte Carlo tree search (MCTS) [2] without repeated oracle calls. On the six QM9 frontier-orbital tasks, SMER-Opt ranks first overall on five tasks, with an 87.95% success rate, an average improvement of  $\Delta y = 2.43$ , and 0.35 min per molecule, about  $7.6\times$  faster than the next-fastest method (Table 3). Our main contributions are summarized as follows:

- SMER is introduced as an edit-response model that predicts the property change caused by each single molecular edit, recasting molecular optimization as a multi-step decision problem driven by fine-grained local supervision rather than endpoint scoring.
- SMER-Opt is introduced as a unified framework that reuses SMER across ranking, prior construction, and value estimation to efficiently navigate multi-step molecular optimization.
- Extensive experiments across multiple tasks and settings demonstrate that SMER-Opt achieves an 87.9% optimization success rate with an average property improvement of  $\Delta y = 2.43$  and a per-molecule search time of only 0.35 minutes.

## 2 Related Work

Unlike molecular property prediction [20] and drug screening [23], which evaluate existing molecules, molecular optimization focuses on modifying lead compounds to generate chemically feasible variants with improved target properties. Recent progress is largely driven by conditional generative modeling: Transformer-based generators directly sample candidates conditioned on target specifications [17], discrete denoising diffusion over molecular graphs improves topology-editing controllability [43], and molecule-specific 3D diffusion further enforces atom and bond consistency as well as geometric constraints [29, 48]. In structure-based drug design, pocket-conditioned variants additionally incorporate binding context to propose binding-compatible ligands [30, 6, 11]. Despite these advances, most generative approaches rely on oracle-in-the-loop search, tying supervision to final molecule outcomes rather than to stepwise, feasibility-aware decisions.

A complementary direction learns from pairs of structurally related molecules rather than generating new ones. Classical matched molecular pair analysis (MMP) extracts interpretable local transformation effects by enumerating matched pairs in large datasets [12, 5], while pairwise delta learning improves data efficiency by predicting property differences between molecular pairs [41, 7]. Although effective under scarce labels, these methods still couple learning signals to endpoints and offer only indirect guidance for selecting the next valid edit.

Both paradigms thus share a fundamental gap: supervision is anchored to whole-molecule outcomes and cannot directly guide the selection of individual structural edits under feasibility constraints. Several dedicated multi-step optimizers address planning more explicitly, including DST via differentiable scaffold trees [8], DyMol via distribution-space guidance [38] and TransDLM via latent-space guidance [47], and CMOMO [45] via conditional multi-objective optimization; yet none explicitly scores individual edits at each step or ties the search signal to the structural feasibility of each individual edit. This motivates a formulation that distills endpoint annotations into process supervision and supports constraint-aware multi-step planning in discrete edit spaces.

## 3 Method

The method comprises two tightly coupled components: SMER predicts the property change induced by a single edit; SMER-Opt composes these local estimates into multi-step trajectories via guided tree search, reusing the same learned signal through two coupled routes: direct prior construction and accumulated path-value estimation.

### 3.1 Problem Definition

We consider single-property molecular optimization under discrete edit actions. Given a starting molecule  $M_0$ , a target property function  $P(\cdot)$ , and an optimization direction  $\sigma \in \{+1, -1\}$  (where  $\sigma = +1$  indicates property increase and  $\sigma = -1$  indicates property decrease), the goal is to find a chemically valid edit sequence  $\tau = (a_0, a_1, \dots, a_{L-1})$  with  $L \leq T$ , such that the optimized molecule  $M_L$  improves the target property as much as possible in the specified direction, where  $T$  is the maximum number of allowed edits. Each edit is applied sequentially through a deterministic

transition operator  $M_{t+1} = \mathcal{T}(M_t, a_t)$ , where  $a_t$  is the edit action, comprising the operation type, location, and parameters.

Not all edits are admissible. For a current molecule  $M_t$ , let  $\mathcal{A}(M_t)$  denote the set of all syntactically generated candidate edits; the feasible action set retains only those candidates whose application yields a chemically valid result:

$$\tilde{\mathcal{A}}(M_t) = \{a \in \mathcal{A}(M_t) \mid \mathcal{V}(\mathcal{T}(M_t, a)) = 1\},$$

where  $\mathcal{V}(\cdot)$  is a binary validity checker, which returns 1 if the resulting molecule passes graph editing, RDKit sanitization, and structural consistency checks. Restricting every step to  $\tilde{\mathcal{A}}$  ensures that all edits along an optimization path remain chemically grounded. The optimization objective is then

$$\tau^* = \arg \max_{\tau: \mathcal{C}(M_0, \tau)=1, |\tau| \leq T} \sigma \left( P(M_{|\tau|}) - P(M_0) \right), \quad (1)$$

where  $\mathcal{C}(M_0, \tau) = 1$  is the path-level feasibility constraint, which requires each action  $a_t$  in the sequence to belong to the corresponding feasible set  $\tilde{\mathcal{A}}(M_t)$ .

To ground the discrete action space, we adopt a molecular graph editing (MGE) representation [54, 35] in which any molecular transformation is decomposed into a sequence of atom-level primitive operations. A structural difference between two molecules is explicitly recovered as an ordered series of local edits rather than treated as an uninterpreted static pair. The main operation types are listed in Table 1. This shared discrete action space serves both stages consistently: at training time, the edit descriptor  $e_i$  is derived from molecule-pair decomposition; at search time, candidate actions are explicitly enumerated and scored at each node.

Table 1: Major operation types of molecular graph editing.

Operation	
① Atom replacement	⑦ Triple bond formation
② Atom addition	⑧ Triple-to-single bond
③ Ring formation	⑨ Add stereochemistry
④ Ring opening	⑩ Remove stereochemistry
⑤ Double bond formation	⑪ Double ring formation
⑥ Double-to-single bond	⑫ Double ring opening

### 3.2 Single-Step Molecular Edit Response Predictor

SMER converts molecule-level property labels into reusable local transition scores by learning to predict the property change  $\hat{\delta}$  induced by each candidate edit directly. Training data are constructed by mining weakly related molecule pairs from a labeled molecular set and decomposing their structural differences into minimal edit units. Each resulting sample is represented as  $\mathcal{D} = \{(M_i^{\text{from}}, M_i^{\text{to}}, e_i, \delta_i)\}_{i=1}^N$ , where  $M_i^{\text{from}}$  and  $M_i^{\text{to}}$  are the molecules before and after a single edit,  $e_i$  is the corresponding edit descriptor,  $N$  is the total number of training samples, and  $\delta_i = P(M_i^{\text{to}}) - P(M_i^{\text{from}})$  is the observed single-step property response. SMER learns a conditional regression function  $\hat{\delta}_i = f_{\Theta}(M_i^{\text{from}}, M_i^{\text{to}}, e_i)$ , which predicts how much the target property will change if edit  $e_i$  is applied in the local structural context of  $M_i^{\text{from}}$ , and  $\Theta = \{\theta_f, \theta_t, \psi, \omega\}$  collects all learnable parameters. Architecturally, SMER uses two geometric molecular encoders: one for the pre-edit molecule and one for the post-edit molecule, together with an edit encoder. This component is illustrated in panel (a) of Figure 2.

Letting  $G^{\text{from}}$  and  $G^{\text{to}}$  denote the 3D molecular graphs of the two molecules, the encoders produce  $h_{\text{from}} = E_{\theta_f}(G^{\text{from}})$ ,  $h_{\text{to}} = E_{\theta_t}(G^{\text{to}})$ , and  $h_e = \phi_{\psi}(e)$ , which are concatenated and passed to a fusion regressor:  $\hat{\delta} = g_{\omega}([h_{\text{from}}; h_{\text{to}}; h_e])$ . where  $E_{\theta_f}$  and  $E_{\theta_t}$  are encoders sharing the same architecture but with independent parameters,  $\phi_{\psi}(\cdot)$  is the edit descriptor encoder, and  $g_{\omega}(\cdot)$  is the fusion regressor. This design explicitly separates the current molecular state, the post-edit molecular state, and the specific edit that caused the transition, giving each factor an independent encoding pathway.

The model is trained by empirical risk minimization:

$$\min_{\Theta} \frac{1}{N} \sum_{i=1}^N \ell(f_{\Theta}(M_i^{\text{from}}, M_i^{\text{to}}, e_i), \delta_i), \quad (2)$$

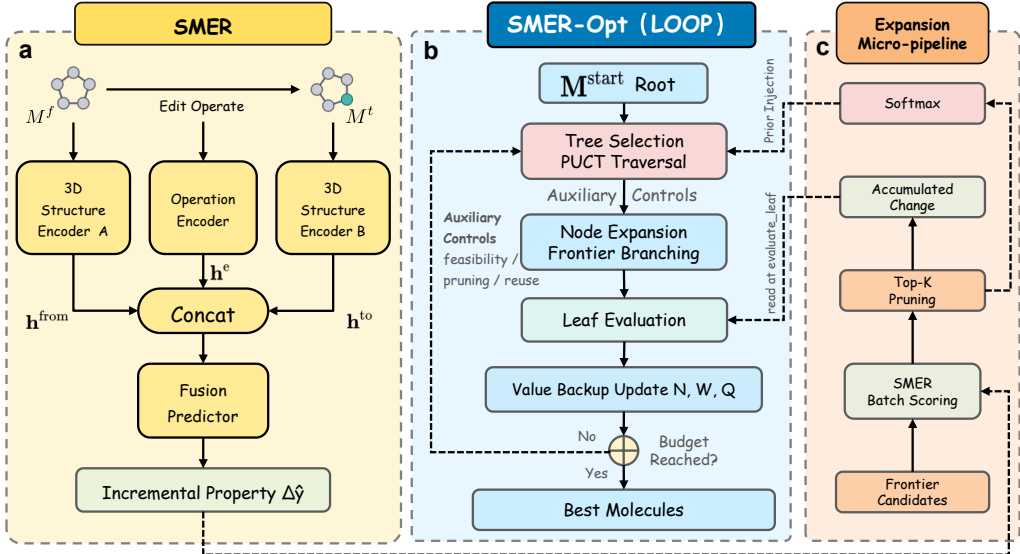


Figure 2: Overview of SMER and SMER-Opt. (a) SMER predicts the single-edit response  $\Delta\hat{y}$ . (b) SMER-Opt uses this response in MCTS for selection, evaluation, and backup. (c) Expansion converts one batch of SMER scores into PUCT priors and accumulated path values.

where  $\ell(\cdot, \cdot)$  is a regression loss such as mean absolute error (MAE) or mean squared error (MSE). After training, SMER provides a reusable local transition score that can be queried for any feasible candidate edit without invoking an external endpoint evaluator.

### 3.3 Tree Search for Multi-Step Molecular Optimization

SMER estimates the response of a single molecular edit, but optimization requires choosing a sequence of edits. The core challenge is that greedy local scoring may close off high-value future paths. SMER-Opt addresses this by embedding SMER into a MCTS planner [16, 2], which evaluates each edit by both its immediate response and its contribution to the multi-step trajectory. The overall search framework is illustrated in panels (b) and (c) of Figure 2.

Each node  $n$  in the search tree corresponds to a molecule  $M_n$  obtained after  $d_n$  edits from the initial molecule. The predicted responses along the path are accumulated as  $G_n = \sum_{k=0}^{d_n-1} \hat{\delta}_k$ , where  $G_n$  is the predicted property shift achieved by the trajectory so far. To make the search objective explicit, we define a path-level utility  $U(G_n) = \sigma G_n$ , where  $\sigma = +1$  for property increase and  $\sigma = -1$  for property decrease. Thus, maximizing  $U(G_n)$  maximizes the signed improvement. Besides  $M_n$ ,  $d_n$ , and  $G_n$ , MCTS maintains standard search statistics: the visit count  $N_n$ , accumulated backup value  $W_n$ , empirical value  $Q_n = W_n/N_n$  after the node has been visited, and a prior  $\pi_n$  used to guide exploration. When node  $n$  is expanded, SMER-Opt first enumerates  $B_n$  chemically valid candidate edits and their resulting molecules:

$$\mathcal{E}(M_n) = \left\{ \left( a_n^{(i)}, M_{n,i}^+ \right) \right\}_{i=1}^{B_n}, \quad M_{n,i}^+ = \mathcal{T} \left( M_n, a_n^{(i)} \right). \quad (3)$$

SMER then scores all candidates in a batch:  $\hat{\delta}_n^{(i)} = f_{\Theta} \left( M_n, M_{n,i}^+, a_n^{(i)} \right)$  for  $i = 1, \dots, B_n$ . Instead of judging an edit only by its one-step response, SMER-Opt scores it by the utility of the trajectory that would result after applying it:  $s_i = U \left( G_n + \hat{\delta}_n^{(i)} \right)$ . For directional optimization, this reduces to ranking candidates by the signed response  $\sigma \hat{\delta}_n^{(i)}$ , since  $G_n$  is shared by all candidates at the same node. Only the top- $K$  candidates are retained, which controls the branching factor while preserving edits that are most aligned with the current search objective. For each retained edit, the corresponding child stores the updated path response  $G_{n_i} = G_n + \hat{\delta}_n^{(i)}$ .

The retained scores are converted into child priors through a softmax transformation,  $\pi_{n_i} = \exp(s_i) / \sum_{j \in \mathcal{R}_n} \exp(s_j)$  for  $i \in \mathcal{R}_n$ , where  $\mathcal{R}_n$  is the retained candidate set and  $n_i$  is the child

generated by candidate  $i$ . During tree traversal, SMER-Opt selects children according to the PUCT rule [34, 39]:

$$\text{PUCT}(n_i) = Q_{n_i} + c \pi_{n_i} \frac{\sqrt{N_n}}{1 + N_{n_i}}, \quad (4)$$

where  $c$  balances exploitation and exploration. The value term prefers branches that have led to high-utility trajectories, whereas the prior term encourages exploration of promising but less visited edits. When a simulation reaches a leaf node  $n_\ell$ , the path is evaluated by the same utility:  $V(n_\ell) = U(G_{n_\ell})$ . This value is backed up along the simulated path: for each node  $u$  on that path,  $N_u \leftarrow N_u + 1$ ,  $W_u \leftarrow W_u + V(n_\ell)$ , and  $Q_u \leftarrow W_u/N_u$ . Branches that become chemically invalid, exceed the maximum depth, or fail to make progress for repeated steps are not expanded further.

In this formulation, each SMER batch-scoring call is reused along two coupled search routes. First, candidate ranking and softmax normalization construct a direct prior for PUCT traversal. Second, the same predicted responses are accumulated into  $G_n$ , which defines the leaf value for backup and final selection. Search terminates when the simulation budget is exhausted, the depth limit  $T$  is reached, or no feasible edit remains. The output molecule is selected from the visited states by maximizing  $U(G_n)$ , yielding a multi-step optimization procedure that is chemically constrained, interpretable, and efficient.

## 4 Experiments

We evaluate SMER and SMER-Opt on QM9 [32], focusing on frontier-orbital properties. SMER is assessed via RMSE, MAE,  $R^2$ , and PCC on HOMO, LUMO, and GAP. SMER-Opt samples 50 test molecules as starting points and reports six optimization tasks covering LUMO, HOMO, and GAP in both increase and decrease directions. Following prior work [8, 45], we set  $\delta_i = y(\hat{m}_i) - y(m_i)$  for increase tasks and  $\delta_i = y(m_i) - y(\hat{m}_i)$  for decrease tasks; primary metrics are Avg Imp =  $\frac{1}{N} \sum_{i=1}^N \delta_i$ , SR =  $\frac{1}{N} |\{i : \delta_i > 0\}|$ , Avg Time, and Overall rank, where Overall rank is obtained by ranking the sum of per-metric ranks and lower values indicate better overall performance. All optimized molecules are evaluated with a PySCF-based quantum-chemistry protocol; Appendix B details this protocol and baseline hyperparameter adaptations. Single-step prediction compares GCN+MLP and GCN+Transformer as 2D backbones against three 3D encoders, Equiformer [24], TensorNet [40], and ViSNet [44]; multi-step optimization baselines include DST [8], DyMol [38], CMOMO [45], and TransDLM [47].

### 4.1 Overall Experiments

We first evaluate whether SMER can provide reliable local transition scores before using it inside tree search. Table 2 compares different molecular encoders under a unified training protocol.

Two conclusions are clear. First, geometric molecular encoders consistently outperform ordinary 2D graph models on this task, indicating that local property responses induced by edits depend strongly on 3D structural context rather than topology alone. Second, across all three properties and all four metrics, ViSNet achieves the best scores, with Equiformer as a close runner-up, confirming ViSNet as the most reliable backbone; it is adopted as the default SMER backbone in subsequent experiments. With the backbone established, we turn to multi-step optimization.

Table 2: Comparison of molecular encoding backbones on the single-step edit response prediction task. Results are averaged over three random seeds. Bold: best; underline: second best.

Property	Method	RMSE↓	MAE↓	$R^2$ ↑	PCC↑
LUMO	GCN <sub>MLP</sub> [15]	0.2220	0.1364	0.9504	0.9749
	GCN <sub>TF</sub> [15, 42]	0.2403	0.1398	0.9437	0.9715
	Equiformer [24]	<u>0.0983</u>	<u>0.0434</u>	<u>0.9905</u>	<u>0.9952</u>
	TensorNet [40]	0.1407	0.0474	0.9804	0.9902
	ViSNet [44]	<b>0.0683</b>	<b>0.0230</b>	<b>0.9953</b>	<b>0.9977</b>
HOMO	GCN <sub>MLP</sub> [15]	0.3878	0.2527	0.8508	0.9224
	GCN <sub>TF</sub> [15]	0.4430	0.2926	0.8055	0.8977
	Equiformer [24]	<u>0.1671</u>	<u>0.0936</u>	<u>0.9724</u>	<u>0.9869</u>
	TensorNet [40]	0.2088	0.1045	0.9573	0.9784
	ViSNet [44]	<b>0.1485</b>	<b>0.0748</b>	<b>0.9782</b>	<b>0.9891</b>
GAP	GCN <sub>MLP</sub> [15]	0.2807	0.1821	0.9224	0.9604
	GCN <sub>TF</sub> [15]	0.2785	0.1797	0.9225	0.9605
	Equiformer [24]	<u>0.1028</u>	<u>0.0607</u>	<u>0.9897</u>	<u>0.9951</u>
	TensorNet [40]	0.1380	0.0791	0.9815	0.9908
	ViSNet [44]	<b>0.0963</b>	<b>0.0328</b>	<b>0.9908</b>	<b>0.9954</b>

Table 3 summarizes performance on six QM9 frontier-orbital tasks. SMER-Opt ranks first on five tasks and is second on HOMO(U), with the best average improvements on LUMO(D) and HOMO(D)

Table 3: Performance on six QM9 frontier-orbital tasks. Each task uses 50 start molecules for decrease(D) or increase(U) optimization. Mean<sub>S</sub>: mean start-molecule property; Avg Imp: mean property change; Suc Rate: fraction of candidates whose change aligns with the target direction; Avg T: per-molecule search time (min); Opt. Mean: mean property of optimized molecules; Overall ranks methods by the summed Avg Imp, Suc Rate, and Avg T ranks. **Bold**: best; underline: second best.

Method	Opt. Mean	Avg Imp↑	Suc Rate↑	Avg T↓	Overall
<b>LUMO (D, Mean<sub>S</sub>=0.459)</b>					
DST [8]	-1.159	1.592	94.58%	2.60	3
DyMol [38]	-2.756	3.215	<b>96.80%</b>	160.20	<u>2</u>
CMOMO [45]	-3.473	<u>3.662</u>	81.39%	35.47	4
TransDLM [47]	-0.006	0.484	63.98%	3.37	5
SMER-Opt (Ours)	-3.682	<b>4.163</b>	93.06%	<b>0.25</b>	<b>1</b>
<b>LUMO (U, Mean<sub>S</sub>=0.459)</b>					
DST	0.975	0.472	35.00%	2.61	4
DyMol	2.756	<b>3.215</b>	<b>96.80%</b>	160.20	<u>2</u>
CMOMO	1.844	<u>1.455</u>	80.00%	27.81	3
TransDLM	0.400	0.106	40.25%	3.37	5
SMER-Opt (Ours)	1.451	1.329	<u>83.13%</u>	<b>0.86</b>	<b>1</b>
<b>HOMO (D, Mean<sub>S</sub>=-7.082)</b>					
DST	-6.656	0.730	73.33%	3.85	3
DyMol	-6.893	0.189	44.40%	215.40	5
CMOMO	-8.459	<u>1.333</u>	<u>92.71%</u>	31.49	<u>2</u>
TransDLM	-6.971	0.117	39.14%	<u>3.37</u>	4
SMER-Opt (Ours)	-8.518	<b>1.559</b>	<b>93.26%</b>	<b>0.06</b>	<b>1</b>
<b>HOMO (U, Mean<sub>S</sub>=-7.082)</b>					
DST	-4.735	<u>2.329</u>	97.71%	3.43	<u>2</u>
DyMol	-5.273	1.809	<b>100.00%</b>	215.40	4
CMOMO	-2.225	<b>4.881</b>	<u>98.68%</u>	30.68	<b>1</b>
TransDLM	-6.754	0.327	70.65%	<u>3.37</u>	5
SMER-Opt (Ours)	-4.936	2.178	95.05%	<b>0.30</b>	<u>2</u>
<b>GAP (D, Mean<sub>S</sub>=7.541)</b>					
DST	4.403	3.207	<u>98.70%</u>	1.64	<u>2</u>
DyMol	3.336	<u>4.268</u>	<b>100.00%</b>	220.20	<u>2</u>
CMOMO	3.316	<b>5.020</b>	68.00%	34.77	4
TransDLM	7.218	0.760	65.55%	2.30	5
SMER-Opt (Ours)	4.066	3.801	94.96%	<b>0.15</b>	<b>1</b>
<b>GAP (U, Mean<sub>S</sub>=7.541)</b>					
DST	7.730	0.091	42.98%	1.81	4
DyMol	7.594	1.391	45.83%	220.20	4
CMOMO	9.387	<b>2.169</b>	<b>87.47%</b>	20.80	<u>2</u>
TransDLM	7.211	0.739	66.46%	2.30	3
SMER-Opt (Ours)	8.010	<u>1.538</u>	<u>68.23%</u>	<b>0.48</b>	<b>1</b>

(4.163 and 1.559). Auxiliary metrics are reported in Appendix A and excluded from the main rankings.

To complement the table-level comparison, Figure 3 visualizes the source and optimized property distributions for the three frontier-orbital objectives. The optimized samples shift toward the requested decrease or increase direction across LUMO, HOMO, and GAP, providing a distribution-level view of the optimization effect achieved by SMER-Opt.

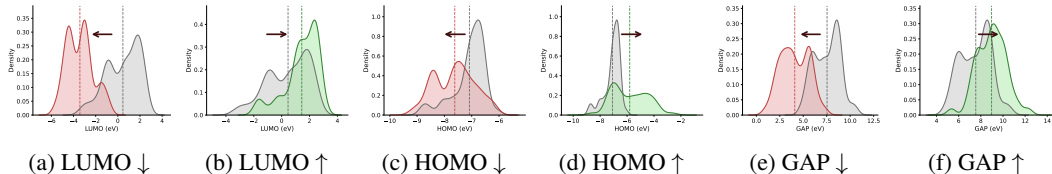


Figure 3: Distribution-level visualization of SMER-Opt optimization effects on QM9 frontier-orbital properties. Gray denotes source molecules, while red and blue denote molecules optimized for the decrease and increase directions, respectively.

Beyond task-level quality, Figure 4 situates SMER-Opt in the efficiency-quality space, showing it achieves competitive average improvement at a fraction of the search time required by CMOMO and DyMol.

To further illustrate the step-by-step reasoning capacity of SMER-Opt, Figure 5 presents two representative optimization trajectories discovered by the MCTS search. In Case 1, the optimizer pursues a decrease objective: starting from CC#CCCCO ( $\Delta_{\text{pred}}=0.00$ ), it first replaces a terminal hydroxyl with fluorine to obtain OCCCC#CF ( $\Delta_{\text{pred}}=-1.09$ , a single-edit gain of 1.09), then performs a compound edit of ring formation followed by atom substitution, arriving at FC#CCC1O01 ( $\Delta_{\text{pred}}=-2.54$ , a two-edit gain of 1.44). The cumulative predicted improvement of 2.54 is achieved in only three atomic-level edits, each step receiving a SMER score consistent with the target direction (i.e., each edit yields a predicted improvement toward the desired decrease), validating the search direction. Case 2 demonstrates an increase objective with a more nuanced trajectory: an initial single-edit substitution yields a small negative change ( $\Delta_{\text{pred}}=-0.12$ ), reflecting a locally unfavorable but globally necessary structural rearrangement; a subsequent three-edit sequence of ring formation, atom substitution, and ring opening then produces a large gain (+3.09), after which a final ring-closure step consolidates the structure with an additional increment of +0.13, reaching a total improvement of +3.10. This non-monotone intermediate step illustrates that SMER-Opt, guided by tree-level value backup, can traverse locally suboptimal edits to reach globally superior molecules, a capability that greedy or beam-search baselines structurally cannot exploit.

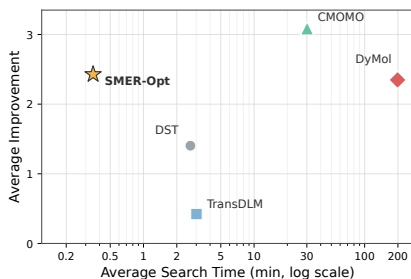


Figure 4: Efficiency-quality trade-off (QM9).

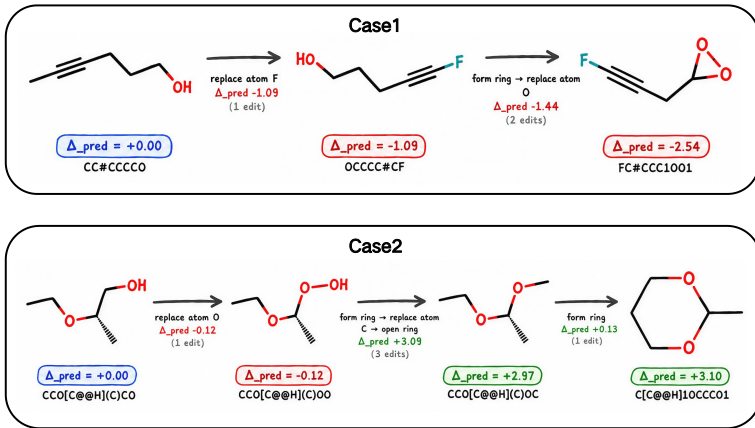


Figure 5: Representative SMER-Opt optimization trajectories on two QM9 molecules. Nodes show molecules and cumulative  $\Delta_{\text{pred}}$ ; edges show edit operations and step gains. Case 1 targets decrease, while Case 2 targets increase with a locally suboptimal intermediate step.

## 4.2 Ablation Studies

**Q1: Does predicting edit-induced property changes outperform predicting absolute post-edit values as the MCTS scoring signal?** To answer this, we compare SMER, which predicts the single-step edit response  $\Delta y$ , against a ViSNet [44] variant that uses the same backbone to predict the absolute post-edit property value inside the same MCTS framework, evaluated on both directions of the dipole moment  $\mu$  task. As shown in Table 4, predicting  $\Delta y$  aligns naturally with MCTS edge-score

Table 4: Scorer formulation ablation on  $\mu$  optimization (50 start molecules,  $\bar{\mu}_{\text{start}} = 2.28$  D). **Bold**: best.

Scorer	$\mu(\text{D})$		$\mu(\text{U})$		Avg Time $\downarrow$ (s/mol)
	Avg Imp $\uparrow$	Suc Rate $\uparrow$	Avg Imp $\uparrow$	Suc Rate $\uparrow$	
ViSNet [44]	1.1988	45.91%	0.4870	16.07%	22.93
SMER (Ours)	<b>1.7780</b>	<b>61.52%</b>	<b>2.6505</b>	<b>86.27%</b>	29.46

semantics, whereas a high-fidelity absolute predictor ( $R^2 = 0.997$ ,  $PCC = 0.999$ ) encodes irrelevant global property variation as noise and consequently fails as a search guidance signal. Per-molecule inference costs are comparable (ViSNet: 22.93 s/mol; SMER: 29.46 s/mol), ruling out computation overhead as a confound.

**Q2: Do tree-structured search and each internal MCTS component contribute independently to optimization performance?** To answer this, we conduct two complementary ablations on HOMO(D) and LUMO(U) with 50 start molecules evaluated under ground-truth assessment. First, we compare SMER-Opt against a BFS variant that retains the same scorer, action space, and chemical constraints but replaces MCTS with breadth-first search, expanding the top- $K$  nodes uniformly at each step without any tree structure or backup mechanisms. Second, within MCTS we ablate three internal components individually: the SMER-derived prior, the leaf-value estimate, and SMER-based expansion ranking (replaced with random top- $K$  retention). As shown in Table 5, SMER-Opt outperforms BFS on both tasks, confirming the necessity of path-level organization. The leaf-value estimate is the most critical internal component: on HOMO(D), removing it drops average improvement from 1.52 to 0.30 and success rate from 91.09% to 36.80%; on LUMO(U), it reduces success rate by 13.00 percentage points. Removing the SMER-derived prior causes only marginal degradation (average improvement changes by less than 0.02 on HOMO(D)), whereas removing expansion ranking leads to a 20.89 percentage point drop in success rate on HOMO(D), indicating that the prior primarily contributes to search efficiency while expansion ranking also affects solution quality.

Table 5: Ablation of search strategy and SMER-Opt internal components on molecular optimization. —: not applicable. **Bold**: best; underline: second best.

Search Strategy	Prior	Leaf Value	Exp. Ranking	HOMO(D)		LUMO(U)	
				Avg Imp $\uparrow$	Suc Rate $\uparrow$	Avg Imp $\uparrow$	Suc Rate $\uparrow$
BFS	—	—	—	0.913	72%	0.473	64%
SMER-Opt (w/o Prior)	$\times$	$\checkmark$	$\checkmark$	<b>1.5384</b>	<u>91.02%</u>	1.2944	79.31%
SMER-Opt (w/o Leaf Value)	$\checkmark$	$\times$	$\checkmark$	0.2988	36.80%	<u>1.2950</u>	69.40%
SMER-Opt (random topK)	$\checkmark$	$\checkmark$	$\times$	1.0698	70.20%	1.2482	66.20%
SMER-Opt	$\checkmark$	$\checkmark$	$\checkmark$	<u>1.5242</u>	<b>91.09%</b>	<b>1.4149</b>	<b>82.40%</b>

### 4.3 Hyperparameter Sensitivity Analysis

We finally examine the robustness of the default search setup on LUMO(D) by varying the search budget, exploration constant, maximum depth, and pruning patience one factor at a time.

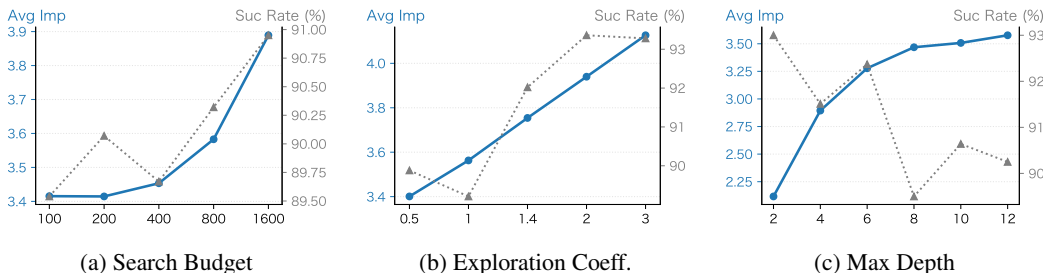


Figure 6: Sensitivity analysis of the core MCTS hyperparameters on LUMO(D).

Figure 6 jointly reports Avg Imp (left axis) and Suc Rate (right axis) for each hyperparameter sweep on LUMO(D). Search budget yields monotonic improvement (Avg Imp 3.41  $\rightarrow$  3.90; Suc Rate 89.5%  $\rightarrow$  91.0%) with diminishing returns beyond 800, making that the cost-effective operating point. The exploration coefficient reveals a pronounced Suc Rate trough at  $c=1$  ( $\approx 89.5\%$ ), which recovers sharply to  $\sim 92\%$  at  $c=1.4$  and saturates near 93% for  $c \geq 2$ ; Avg Imp increases nearly linearly from 3.40 at  $c=0.5$  to 4.10 at  $c=3$ . The trough at  $c=1$  shows that a UCB coefficient of 1 provides insufficient exploration, confining the search to a narrow region of chemical space, while coefficients in  $[1.4, 2]$  achieve near-peak success rate alongside strong Avg Imp. Maximum depth increases Avg Imp from 2.15 at depth 2 to 3.56 at depth 12, with most gains already captured at depth 6 (3.30); Suc Rate follows the opposite trajectory, peaking near 93% at depth 2, declining to a

trough of  $\approx 89.8\%$  at depth 8, and only partially recovering thereafter. These opposing trends reflect the inherent tension in molecular graph editing between reaching high-improvement molecules via longer edit chains and maintaining structural proximity to the start molecule; depth 6 resolves this trade-off competitively. Pruning patience has negligible effect across all tested values, confirming that the SMER-based pruning criterion is already sufficiently conservative. Default values are listed in Appendix C.

## 5 Conclusion

To enable efficient and principled multi-step molecular property optimization through fine-grained, action-level supervision, we propose SMER and SMER-Opt, a two-level framework that decomposes molecule-level property supervision into action-level edit-response prediction of  $\Delta y$  and MCTS-guided multi-step trajectory optimization. Evaluated on QM9 across six frontier-orbital tasks, SMER-Opt ranks first in five of six tasks on the combined metric, achieving the highest weighted success rate of 87.95% at only 21 seconds, or 0.35 min, per molecule, roughly  $7.6\times$  faster than DST and  $86\times$  faster than CMOMO, demonstrating that principled multi-step molecular optimization need not sacrifice efficiency. Nevertheless, the current framework is trained on small-molecule datasets, and its generalization to larger or more structurally complex molecules remains unexplored. Future work will extend SMER-Opt to multi-objective settings and replace its heuristic guidance with a reinforcement-learning-trained policy.

## A Auxiliary Reference Metrics

This section provides the full definitions of the five auxiliary reference metrics mentioned in Section 4, together with the detailed per-task results. These metrics are not used in the main ranking, but collectively characterize the trade-off among optimization strength, structural retention, diversity, and chemical plausibility from complementary perspectives.

- **logP** [25]: the octanol/water partition coefficient, used as a proxy for drug-likeness and membrane permeability; the empirically favorable range is  $[0, 5]$ .
- **Ring count**: the total number of rings in the optimized molecule; excessively large values (e.g.  $> 4$ ) often indicate over-complexification of the scaffold.
- **HamDiv** [10]: a Hamiltonian-circuit-based diversity measure over the set of candidate molecules returned by a method; higher values indicate a more dispersed candidate pool (range  $[0, 1]$ ).
- **Morgan similarity** [33]: Tanimoto similarity between the ECFP4 fingerprint of the optimized molecule and that of the starting molecule; higher values indicate greater structural proximity to the starting point (range  $[0, 1]$ ; a reasonable structural-retention range is approximately  $[0.3, 0.7]$ ).
- **GED similarity** [36, 9]: normalized graph-edit-distance similarity between the optimized molecule and the starting molecule; higher values indicate smaller structural divergence (range  $[0, 1]$ ).

Table 6 reports these metrics for all methods across the six QM9 frontier-orbital optimization tasks.

## B Unified Property Evaluation and Baseline Hyperparameters

### B.1 Unified PySCF Evaluation Protocol

To make the multi-step molecular optimization results comparable across methods, we evaluate all generated molecules with the same quantum-chemical protocol for HOMO, LUMO, and HOMO–LUMO gap. The core electronic-structure backend is PySCF, using its molecular-construction module `pyscf.gto` and DFT module `pyscf.dft`; RDKit is used for three-dimensional conformer generation, and ASE is used for atomistic structure representation during geometry preparation. For each molecule, an initial 3D conformation is generated from SMILES by RDKit ETKDG with random seed 42, followed by MMFF94 force-field minimization. The optimized geometry is then used to construct a PySCF molecular object with neutral charge. We perform DFT calculations at the B3LYP/6-31G(2df,p) level of theory, using restricted Kohn–Sham (RKS) calculations for closed-shell molecules and unrestricted Kohn–Sham (UKS) calculations when an open-shell configuration is required. The SCF convergence threshold is set to  $10^{-10}$  Hartree and the DFT integration grid level is set to 4. HOMO and LUMO energies are extracted from the converged molecular orbital energies and occupation numbers, and the gap is computed as  $\epsilon_{\text{LUMO}} - \epsilon_{\text{HOMO}}$ . This protocol follows the QM9-style frontier-orbital evaluation setting to ensure direct comparability across methods.

Table 7 summarizes the key hyperparameters used by the unified PySCF evaluator.

This protocol is used as a post-generation evaluator. It does not modify the internal search or generation mechanism of a baseline unless the original objective oracle must be adapted from its released task to HOMO, LUMO, or GAP optimization. The purpose is therefore to standardize the final property measurement rather than to introduce an additional advantage for any particular method.

### B.2 Baseline Hyperparameter Adaptations

For baseline methods, we use the released implementation defaults whenever possible, modifying settings only to adapt each method to the QM9 frontier-orbital tasks, to run all methods on the same start-molecule set, or to keep the PySCF-based evaluation cost tractable. CMOMO: population size reduced from 100 to 50, total iterations from 100 to 3, stage-1 iterations from 50 to 2; start set restricted to the first 50 QM9 test molecules; QED/logP objectives replaced by HOMO/LUMO/GAP.

Table 6: Auxiliary reference metrics on molecular property optimization tasks. These metrics are reported for interpretation only and are not used in the main ranking.

Method	logP	Rings	HamDiv	Morgan	GED
<b>LUMO (D, <math>S=0.459</math>)</b>					
DST [8]	1.943	5.271	6.648	0.222	0.297
DyMol [38]	3.117	10.000	8.009	0.051	0.073
CMOMO [45]	0.426	6.980	6.209	0.116	0.158
TransDLM [47]	0.420	1.490	1.120	0.461	0.547
SMER-Opt (Ours)	0.082	1.820	1.704	0.071	0.145
<b>LUMO (U, <math>S=0.459</math>)</b>					
DST	2.032	4.813	6.549	0.240	0.325
DyMol	3.117	10.000	8.009	0.051	0.073
CMOMO	1.265	5.520	5.515	0.124	0.141
TransDLM	0.571	1.480	1.146	0.489	0.551
SMER-Opt (Ours)	1.293	2.460	2.354	0.154	0.153
<b>HOMO (D, <math>S=-7.082</math>)</b>					
DST	1.471	5.333	6.722	0.300	0.385
DyMol	2.306	10.000	8.168	0.063	0.085
CMOMO	0.751	6.520	6.925	0.110	0.161
TransDLM	0.400	1.580	1.302	0.485	0.551
SMER-Opt (Ours)	0.713	2.760	3.308	0.166	0.215
<b>HOMO (U, <math>S=-7.082</math>)</b>					
DST	1.552	5.917	6.869	0.205	0.264
DyMol	3.242	10.000	8.491	0.051	0.087
CMOMO	-0.121	9.040	8.341	0.079	0.126
TransDLM	0.571	1.660	1.274	0.456	0.545
SMER-Opt (Ours)	0.048	2.360	2.607	0.170	0.194
<b>GAP (D, <math>S=7.541</math>)</b>					
DST	1.000	3.200	5.333	0.296	0.391
DyMol	3.880	9.000	7.833	0.045	0.073
CMOMO	0.750	7.612	7.097	0.093	0.179
TransDLM	0.535	3.063	1.988	0.492	0.554
SMER-Opt (Ours)	0.076	2.932	3.335	0.096	0.158
<b>GAP (U, <math>S=7.541</math>)</b>					
DST	0.836	3.340	5.426	0.465	0.456
DyMol	1.435	10.000	8.274	0.162	0.213
CMOMO	1.196	5.500	6.696	0.119	0.179
TransDLM	0.532	2.833	1.784	0.484	0.549
SMER-Opt (Ours)	1.602	2.540	3.466	0.141	0.180

These reductions are motivated by the high cost of quantum-chemical evaluation: each PySCF call (involving the `gto`, `dft`, and `lib` modules) carries a per-step wall-clock cost substantially higher than that of QED or logP, and the original configuration of 100 individuals over 100 generations would result in an infeasible total runtime. Experiments show that the 3-generation, 50-individual configuration preserves the optimization effectiveness of CMOMO while reducing the total runtime substantially relative to the original hyperparameters. DST: oracle budget set to 10 calls per start molecule; DPP candidate selection truncated to at most  $10\times$  the population size; other defaults (generations, population size, runs per molecule) kept. DyMol and TransDLM: only task-specific switches (target property, dataset, and start-molecule range) were set; all other hyperparameters, including model architectures and training settings, follow the corresponding released implementation defaults.

Table 7: Key hyperparameters of the unified PySCF evaluator.

Hyperparameter	Value
DFT level of theory	B3LYP/6-31G(2df,p)
DFT integration grid level	4
SCF convergence threshold	$10^{-10}$ Hartree
Conformer initialization	RDKit ETKDG, random seed 42
Geometry pre-optimization	MMFF94
Kohn–Sham treatment	RKS for closed-shell; UKS for open-shell cases
Molecular charge	Neutral
Closed-shell spin	0

## C Default Implementation Configuration

Table 8 summarizes the default implementation settings used throughout our experiments. These values correspond to the representative configuration adopted for the final reported results, unless a specific ablation or sensitivity study states otherwise. We include them here to make the empirical setup more transparent and to facilitate reproducibility.

The configuration consists of two parts. The SMER block specifies the architectural choices of the single-step molecular edit response predictor, including the hidden dimensionality, the depth of geometric message passing, the radial basis expansion size, the interaction cutoff, and the layer structures used by the molecule projector, operation encoder, and fusion head. Together, these hyperparameters determine how local geometric context and edit descriptors are encoded before response regression.

The MCTS block reports the default search settings used by SMER-Opt, including the simulation budget, the exploration weight in tree policy, the maximum search depth, the pruning patience, and the branching cap retained at each expansion step. These values were chosen as stable defaults for balancing optimization quality and computational cost, and they are consistent with the sensitivity analysis discussed in Section 4.

Table 8: Default implementation configurations for SMER and MCTS.

Category	Parameter	Default	Description
SMER	Hidden dim (hidden_channels)	128	Geometric encoder hidden dimension
SMER	#Layers (num_layers)	6	Number of geometric message passing layers
SMER	#Radial basis (num_rbf)	32	Number of radial basis functions
SMER	Cutoff radius (cutoff)	5.0	Radius graph cutoff distance
SMER	Molecule projector	64-128-256-256	Molecular representation projection layers
SMER	Edit feature dim (edit_dim)	15	Edit operation feature dimension
SMER	Operation encoder	15-64-128-256	Edit condition encoding layers
SMER	Fusion head	1280-512-256-128-1	Joint regression head structure
MCTS	Simulations (num_simulations)	800	Default search budget
MCTS	Exploration weight	2.0	Exploration coefficient in tree policy
MCTS	Max depth	10	Maximum editing depth
MCTS	Pruning patience	3	Patience for stagnation pruning
MCTS	Max branching	10	Upper bound of retained candidates per expansion

## D Compute Resources

All SMER training and SMER-Opt inference experiments were conducted on a single NVIDIA RTX A6000 GPU (48 GB VRAM). SMER was trained with a batch size of 512 for approximately 5 hours of wall-clock time on this hardware. SMER-Opt inference is CPU-bound (dominated by the per-step PySCF quantum-chemistry evaluations) and does not require a GPU at test time.

## References

- [1] Emmanuel Bengio, Moksh Jain, Maksym Korablyov, Doina Precup, and Yoshua Bengio. Flow network based generative models for non-iterative diverse candidate generation. *Advances in neural information processing systems*, 34:27381–27394, 2021.
- [2] Cameron B Browne, Edward Powley, Daniel Whitehouse, Simon M Lucas, Peter I Cowling, Philipp Rohlfshagen, Stephen Tavener, Diego Perez, Spyridon Samothrakis, and Simon Colton. A survey of monte carlo tree search methods. *IEEE Transactions on Computational Intelligence and AI in games*, 4(1):1–43, 2012.
- [3] Jiameng Chen, Xiantao Cai, Jia Wu, and Wenbin Hu. Antibody design and optimization with multi-scale equivariant graph diffusion models for accurate complex antigen binding. In James Kwok, editor, *Proceedings of the Thirty-Fourth International Joint Conference on Artificial Intelligence, IJCAI-25*, pages 2722–2730. International Joint Conferences on Artificial Intelligence Organization, 8 2025. Main Track.
- [4] Xiangsen Chen, Ruilong Wu, Yanyan Lan, Ting Ma, and Yang Liu. Molevolve: Llm-guided evolutionary search for interpretable molecular optimization. *arXiv preprint arXiv:2603.24382*, 2026.
- [5] Alexander G Dosseter, Edward J Griffen, and Andrew G Leach. Matched molecular pair analysis in drug discovery. *Drug Discovery Today*, 18(15-16):724–731, 2013.
- [6] Wei Feng, Lvwei Wang, Zaiyun Lin, Yanhao Zhu, Han Wang, Jianqiang Dong, Rong Bai, Huting Wang, Jielong Zhou, Wei Peng, et al. Generation of 3d molecules in pockets via a language model. *Nature Machine Intelligence*, 6(1):62–73, 2024.
- [7] Zachary Fralish, Ashley Chen, Paul Skaluba, and Daniel Reker. Deepdelta: predicting admet improvements of molecular derivatives with deep learning. *Journal of cheminformatics*, 15(1):101, 2023.
- [8] Tianfan Fu, Wenhao Gao, Cao Xiao, Jacob Yasonik, Connor W Coley, and Jimeng Sun. Differentiable scaffolding tree for molecular optimization. *arXiv preprint arXiv:2109.10469*, 2021.
- [9] Xinbo Gao, Bing Xiao, Dacheng Tao, and Xuelong Li. A survey of graph edit distance. *Pattern Analysis and applications*, 13(1):113–129, 2010.
- [10] Xiuyuan Hu, Guoqing Liu, Quanming Yao, Yang Zhao, and Hao Zhang. Hamiltonian diversity: effectively measuring molecular diversity by shortest hamiltonian circuits. *Journal of Cheminformatics*, 16(1):94, 2024.
- [11] Lei Huang, Tingyang Xu, Yang Yu, Peilin Zhao, Xingjian Chen, Jing Han, Zhi Xie, Hailong Li, Wenge Zhong, Ka-Chun Wong, and Hengtong Zhang. A dual diffusion model enables 3d molecule generation and lead optimization based on target pockets. *Nature Communications*, 15:2657, 2024.
- [12] Jameed Hussain and Ceara Rea. Computationally efficient algorithm to identify matched molecular pairs (mmps) in large data sets. *Journal of chemical information and modeling*, 50(3):339–348, 2010.
- [13] Wengong Jin, Regina Barzilay, and Tommi Jaakkola. Junction tree variational autoencoder for molecular graph generation. In *Proceedings of the 35th International Conference on Machine Learning*, volume 80, pages 2323–2332. PMLR, 2018.
- [14] Hyeonah Kim, Minsu Kim, Sanghyeok Choi, and Jinkyoo Park. Genetic-guided gflownets for sample efficient molecular optimization. *Advances in Neural Information Processing Systems*, 37:42618–42648, 2024.
- [15] Thomas N. Kipf and Max Welling. Semi-supervised classification with graph convolutional networks. In *International Conference on Learning Representations*, 2017.
- [16] Levente Kocsis and Csaba Szepesvári. Bandit based monte-carlo planning. In *European conference on machine learning*, pages 282–293. Springer, 2006.
- [17] Deqian Kong, Yuhao Huang, Jianwen Xie, Edouardo Honig, Ming Xu, Shuanghong Xue, Pei Lin, Sanping Zhou, Sheng Zhong, Nanning Zheng, et al. Molecule design by latent prompt transformer. *Advances in Neural Information Processing Systems*, 37:89069–89097, 2024.
- [18] Michał Koziarski, Andrei Rekes, Dmytro Shevchuk, Almer van der Sloot, Piotr Gaiński, Yoshua Bengio, Chenghao Liu, Mike Tyers, and Robert Batey. Rgfn: Synthesizable molecular generation using gflownets. *Advances in Neural Information Processing Systems*, 37:46908–46955, 2024.
- [19] Kun Li, Xiuwen Gong, Shirui Pan, Jia Wu, Bo Du, and Wenbin Hu. Regressor-free molecule generation to support drug response prediction. *arXiv preprint arXiv:2405.14536*, 2024.

- [20] Kun Li, Longtao Hu, Jiameng Chen, Hongzhi Zhang, Yida Xiong, Xiantao Cai, Wenbin Hu, and Jia Wu. Can molecular evolution mechanism enhance molecular representation? *Proceedings of the AAAI Conference on Artificial Intelligence*, 40(18):15108–15116, Mar. 2026.
- [21] Kun Li, Zhennan Wu, Shoupeng Wang, Jia Wu, Shirui Pan, and Wenbin Hu. Drugpilot: Llm-based parameterized reasoning agent for drug discovery. *arXiv preprint arXiv:2505.13940*, 2025.
- [22] Kun Li, Yida Xiong, Hongzhi Zhang, Xiantao Cai, Jia Wu, Bo Du, and Wenbin Hu. Graph-structured small molecule drug discovery through deep learning: Progress, challenges, and opportunities. In *2025 IEEE International Conference on Web Services (ICWS)*, pages 1033–1042, 2025.
- [23] Kun Li, Yue Zeng, Yi-da Xiong, Hao-chen Wu, Sui Fang, Zhi-yan Qu, Yan Zhu, Bo Du, Zhao-bing Gao, and Wen-bin Hu. Contrastive learning-based drug screening model for glun1/glun3a inhibitors. *Acta Pharmacologica Sinica*, pages 1–13, 2025.
- [24] Yi-Lun Liao and Tess Smidt. Equiformer: Equivariant graph attention transformer for 3D atomistic graphs. In *International Conference on Learning Representations*, 2023.
- [25] Christopher A Lipinski, Franco Lombardo, Beryl W Dominy, and Paul J Feeney. Experimental and computational approaches to estimate solubility and permeability in drug discovery and development settings. *Advanced drug delivery reviews*, 23(1-3):3–25, 1997.
- [26] Meng Liu, Keqiang Yan, Bora Oztekin, and Shuiwang Ji. GraphEBM: Molecular graph generation with energy-based models. In *Energy-Based Models Workshop, ICLR*, 2021.
- [27] Luca Miglior, Lorenzo Simone, Marco Podda, and Davide Bacciu. Towards efficient molecular property optimization with graph energy based models, 2025.
- [28] Matteo Ninniri, Marco Podda, and Davide Bacciu. Graph diffusion that can insert and delete. *Advances in Neural Information Processing Systems*, 38:78375–78401, 2026.
- [29] Xingang Peng, Jiaqi Guan, Qiang Liu, and Jianzhu Ma. MolDiff: Addressing the atom-bond inconsistency problem in 3D molecule diffusion generation. In Andreas Krause, Emma Brunskill, Kyunghyun Cho, Barbara Engelhardt, Sivan Sabato, and Jonathan Scarlett, editors, *Proceedings of the 40th International Conference on Machine Learning*, volume 202 of *Proceedings of Machine Learning Research*, pages 27611–27629. PMLR, 23–29 Jul 2023.
- [30] Xingang Peng, Shitong Luo, Jiaqi Guan, Qi Xie, Jian Peng, and Jianzhu Ma. Pocket2mol: Efficient molecular sampling based on 3d protein pockets. In *International conference on machine learning*, pages 17644–17655. PMLR, 2022.
- [31] Xiaohan Qin, Chao Wang, Zhengyang Zhou, Linjiang Chen, Wenjie Du, and Yang Wang. Msanchor: De novo molecular generation from mass spectrometry data with anchor-extended molecular scaffolds. In *Proceedings of the AAAI Conference on Artificial Intelligence*, volume 40, pages 953–961, 2026.
- [32] Raghunathan Ramakrishnan, Pavlo O Dral, Matthias Rupp, and O Anatole Von Lilienfeld. Quantum chemistry structures and properties of 134 kilo molecules. *Scientific data*, 1(1):1–7, 2014.
- [33] David Rogers and Mathew Hahn. Extended-connectivity fingerprints. *Journal of chemical information and modeling*, 50(5):742–754, 2010.
- [34] Christopher D Rosin. Multi-armed bandits with episode context. *Annals of Mathematics and Artificial Intelligence*, 61(3):203–230, 2011.
- [35] Mikołaj Sacha, Mikołaj Błaż, Piotr Byrski, Paweł Dąbrowski-Tumański, Mikołaj Chromiński, Rafał Loska, Paweł Włodarczyk-Pruszyński, and Stanisław Jastrzębski. Molecule edit graph attention network: Modeling chemical reactions as sequences of graph edits. *Journal of Chemical Information and Modeling*, 61(7):3273–3284, 2021.
- [36] Alberto Sanfeliu and King-Sun Fu. A distance measure between attributed relational graphs for pattern recognition. *IEEE Transactions on Systems, Man, and Cybernetics*, 13(3):353–362, 1983.
- [37] Chence Shi, Minkai Xu, Zhaocheng Zhu, Weinan Zhang, Ming Zhang, and Jian Tang. GraphAF: A flow-based autoregressive model for molecular graph generation. In *International Conference on Learning Representations*, 2020.
- [38] Dong-Hee Shin, Young-Han Son, Ji-Wung Han, Tae-Eui Kam, et al. Dymol: Dynamic many-objective molecular optimization with objective decomposition and progressive optimization. In *ICLR 2024 Workshop on Generative and Experimental Perspectives for Biomolecular Design*, 2024.

- [39] David Silver, Julian Schrittwieser, Karen Simonyan, Ioannis Antonoglou, Aja Huang, Arthur Guez, Thomas Hubert, Lucas Baker, Matthew Lai, Adrian Bolton, et al. Mastering the game of go without human knowledge. *Nature*, 550(7676):354–359, 2017.
- [40] Guillem Simeon and Gianni De Fabritiis. TensorNet: Cartesian tensor representations for efficient learning of molecular potentials. In *Advances in Neural Information Processing Systems*, 2023.
- [41] Michael Tynes, Wenhao Gao, Daniel J Burrill, Enrique R Batista, Danny Perez, Ping Yang, and Nicholas Lubbers. Pairwise difference regression: a machine learning meta-algorithm for improved prediction and uncertainty quantification in chemical search. *Journal of chemical information and modeling*, 61(8):3846–3857, 2021.
- [42] Ashish Vaswani, Noam Shazeer, Niki Parmar, Jakob Uszkoreit, Llion Jones, Aidan N Gomez, Łukasz Kaiser, and Illia Polosukhin. Attention is all you need. In *Advances in Neural Information Processing Systems*, volume 30, 2017.
- [43] Clement Vignac, Igor Krawczuk, Antoine Siraudin, Bohan Wang, Volkan Cevher, and Pascal Frossard. Digress: Discrete denoising diffusion for graph generation. In *The Eleventh International Conference on Learning Representations*, 2023.
- [44] Yusong Wang, Tong Wang, Shaoning Li, Xinheng He, Mingyu Li, Zun Wang, Nanning Zheng, Bin Shao, and Tie-Yan Liu. Enhancing geometric representations for molecules with equivariant vector-scalar interactive message passing. *Nature Communications*, 15(1):313, Jan 2024.
- [45] Xin Xia, Yajie Zhang, Xiangxiang Zeng, Xingyi Zhang, Chunhou Zheng, and Yansen Su. CMOMO: a deep multi-objective optimization framework for constrained molecular multi-property optimization. *Briefings in Bioinformatics*, 26(4):bbaf335, 2025.
- [46] Hongxin Xiang, Jun Xia, Xin Jin, Wenjie Du, Li Zeng, and Xiangxiang Zeng. Electron density-enhanced molecular geometry learning. In *Proceedings of the Thirty-Fourth International Joint Conference on Artificial Intelligence*, pages 7840–7848, 2025.
- [47] Yida Xiong, Kun Li, Jiameng Chen, Hongzhi Zhang, Di Lin, Yan Che, and Wenbin Hu. Text-guided multi-property molecular optimization with a diffusion language model. *Information Fusion*, page 103907, 2025.
- [48] Minkai Xu, Alexander S Powers, Ron O Dror, Stefano Ermon, and Jure Leskovec. Geometric latent diffusion models for 3d molecule generation. In *International Conference on Machine Learning*, pages 38592–38610. PMLR, 2023.
- [49] Jiaxuan You, Bowen Liu, Zhitao Ying, Vijay Pande, and Jure Leskovec. Graph convolutional policy network for goal-directed molecular graph generation. *NeurIPS*, 31, 2018.
- [50] Jiajun Yu, Zhihao Wu, Jinyu Cai, Adele Lu Jia, and Jicong Fan. Kernel readout for graph neural networks. In *IJCAI*, pages 2505–2514, 2024.
- [51] Jiajun Yu, Zhihao Wu, Jielong Lu, Tianyue Wang, and Haishuai Wang. A centrality-based graph learning framework. In *Proceedings of the Thirty-Fourth International Joint Conference on Artificial Intelligence*, pages 3588–3596, 2025.
- [52] Jiajun Yu, Yizhen Zheng, Huan Yee Koh, Shirui Pan, Tianyue Wang, and Haishuai Wang. Collaborative expert llms guided multi-objective molecular optimization. *arXiv preprint arXiv:2503.03503*, 2025.
- [53] Yizhen Zheng, Huan Yee Koh, Jiabin Ju, Madeleine Yang, Lauren T May, Geoffrey I Webb, Li Li, Shirui Pan, and George Church. Large language models for drug discovery and development. *Patterns*, 6(10), 2025.
- [54] Wenpin Zhong, Zhenyang Yang, and Chen-Yang Chen. Retrosynthesis prediction using an end-to-end graph generative architecture for molecular graph editing. *Nature Communications*, 14(1):3009, 2023.
- [55] Xiangxin Zhou, Xiwei Cheng, Yuwei Yang, Yu Bao, Liang Wang, and Quanquan Gu. Decompt: Controllable and decomposed diffusion models for structure-based molecular optimization. In *International Conference on Learning Representations*, 2024.
- [56] Zhenpeng Zhou, Steven Kearnes, Li Li, Richard N Zare, and Patrick Riley. Optimization of molecules via deep reinforcement learning. *Scientific reports*, 9(1):10752, 2019.